Experiments on free decay of quasi-two-dimensional turbulent flows

S. Danilov, F. V. Dolzhanskii, V. A. Dovzhenko, and V. A. Krymov

Institute of Atmospheric Physics, 3 Pyzhevsky per., 109017 Moscow, Russia

Decaying quasi-two-dimensional turbulence in a thin-layer flow is explored in laboratory experiments. We report the presence of power-law interval in the enstrophy decay law, in agreement with earlier experiments by Cardoso *et al.* [Phys. Rev. E **49**, 454 (1994)] and Hansen *et al.* [Phys. Rev. E **58**, 7261 (1998)]. The decay exponent proves sensitive to the way in which the energy decay is compensated. For the range of initial microscale Reynolds numbers between 35 and 95, the decay exponent is close to -0.4 for the ratio of enstrophy to energy, and to -0.75 for the enstrophy multiplied with a compensating factor of $\exp(-2\lambda t)$, where λ is the bottom-drag coefficient and t the decay time. The vorticity behavior does not comply with the theory of Carnevale *et al.* [Phys. Rev. Lett. **66**, 2735 (1991)]: robust vortices are not observed in the vorticity field and the vorticity kurtosis is less than the Gaussian value.

I. INTRODUCTION

As follows from numerical simulations, the decay of two-dimensional (2D) incompressible turbulence at high initial Reynolds numbers proceeds via the formation of vortices [1–7]. The vortices are stable against the background shear and are not stirred, which results in suppression of enstrophy dissipation. The enstrophy decay law is generally shallower than Batchelor's t^{-2} law [8]. Existing theories [3–6,9,10] predict a variety of scenarios for the decay and the basic question is whether they can be observed in real flows.

Motivated by numeric evidence, Carnevale *et al.* [3] (see also [2,4]) assumed that not only energy, but also the vorticity extremum is conserved as 2D turbulence decays. Their scaling predicts that if the number of vortices decreases as $t^{-\xi}$, the enstrophy decays as $t^{-\xi/2}$, vortex size grows as $t^{\xi/4}$, and both the distance between vortices and vorticity kurtosis as $t^{\xi/2}$. The numerically measured value of the exponent ξ is 0.71–0.75 [2–4], and recent simulations at very fine resolution in Ref. [7] give ξ between 0.73 and 0.77. Hansen *et al.* [11] claim to have experimental support to this scenario in their laboratory simulations of thin-layer flows showing that $\xi = 0.7 \pm 0.1$ and that the number of vortices, the enstrophy, the vortex size, the distance between vortices and vorticity kurtosis all follow power laws with properly related exponents. In particular, they found the exponent of -0.47 for the enstrophy decay.

Numerical experiments in Refs. [3,4] as well as those in Refs. [5,6] suggest that the decay of 2D turbulence can be viewed as going through interactions between separate vortices.

However, according to simulations of [9], the enstrophy decays as $t^{-1.2}$ in runs with ordinary viscosity and as $t^{-0.4}$ in runs with hyperviscosity. While the latter result is close to the results of [2–4], the former is much steeper thus pointing out to the sensitivity of the enstrophy decay to the type of small-scale dissipation. Chasnov [10] studied the decay in runs with ordinary viscosity and found the decay law to be sensitive to the initial Reynolds number. According to Ref. [10], the exponent of the enstrophy decay varies from approximately -2 at the critical initial Reynolds number of

approximately 15.73 to -0.8 in the limit of high Reynolds numbers (the Reynolds number is defined below). These results imply that decay laws depend on enstrophy dissipation mechanism and the Reynolds number.

Quantitative laboratory experiments on the behavior of decaying 2D turbulence are few in number. Experiments using soap-film setups explored spectra and velocity and vorticity increments in turbulence evolving downstream a comb [12–18]. Energy spectra were found to scale with wave number as $k^{-3.3}$ in Refs. [12,13,15]. The external scale of turbulence was shown to evolve linearly with time [13] and structure functions of velocity and vorticity were found to behave in general agreement with the theoretical predictions [14–16]. The velocity measurements in Refs. [12,13,15,16] were carried out with velocimeters and Taylor's hypothesis was invoked to link the frequency spectra at a given point to the spatial spectra. The performance of this hypothesis was analyzed in Ref. [18]. Particle image velocimetry (PIV) methods were used in Refs. [14,17]. Paper [13] pays attention to the fact that flows in soap-film experiments experience a drag against surrounding air, while paper [17] demonstrates that this drag could be parametrized via the Rayleigh term added to 2D Navier-Stokes equations.

Decay laws of 2D turbulence are analyzed in Refs. [11,19]. These experiments use electromagnetic forcing to excite vortex flows in thin layers of weakly conducting liquid and PIV methods to recover the velocity field on a regular grid. In experiments [11] a special two-layer setup is used to reduce the magnitude of divergent component in thin-layer flows. The interface between layers of slightly different density is impermeable to fluid particles. This suppresses circulation in a vertical plane and, consequently, horizontal divergence. 2D turbulence in thin-layer flows is affected by bottom friction, which is usually parametrized via Rayleigh friction term [20]. In this respect flows excited electromagnetically in thin layers and flows in soap films are similar, and distinct from decaying flows simulated in numerical experiments.

While there is no definite conclusion on the preferable decay scenario in Ref. [19], where the ratio of enstrophy to energy was found to behave as $t^{-0.44}$, the results of [11] seem to support that of [3], if properly interpreted. However,

the systems studied in [3] and that used in [11] differ considerably (in initial conditions, the type of small-scale dissipation and the presence of bottom drag in the laboratory flow) and one may wonder whether there are grounds for such coincidence.

The study presented below uses the experimental setup similar to that of [11,19]. We used a single layer setup assuming that small (though higher than in [11]) velocity divergence existing in this case will not change the laws of decay considerably (compare laws in [11,19] where two-layer and single-layer setups are used).

Our goal is to measure the enstrophy decay exponents, compare them to exponents found in numerical simulations and in [11,19], and analyze to what extent the decay complies with the known theories. Despite our experiments and those of [11,19] deal with similar flows, and lead to close values of the enstrophy decay exponent if the latter is measured in the same way, we conclude that decay in thin-layer flows explored by us does not lend support to decay theories derived from numerical simulations.

II. THE EXPERIMENTAL PROCEDURE AND RESULTS

A. Experimental procedure

The experimental setup consists of a rectangular cell with a thin bottom, the array of magnets with vertical magnetization axis, placed under the cell's bottom, and a pair of electrodes aligned with the cell vertical walls and connected to the power supply. The horizontal dimensions of the cell are 14×40 cm^2. We used cylindrical magnets of 14 mm in diameter and of 6 mm in height. Magnets formed a doubly periodic lattice with alternating direction of magnetization. The cell was filled with a weak solution of blue vitriol to the depth h (we varied it from 2 to 6 mm). The electric current exciting the initial flow was varied from 0.1 A to 3 A. In our experiments, we let the flow reach a statistically quasistationary regime. Then the electric current was switched off (at some "zero" moment of time $t = t_0$), and the decay of the flow was recorded for time interval long enough for the flow to come to rest.

The velocity fields were recovered with a variant of PIV method. The working area of the flow was a rectangular with sides of 140×185 mm^2. The surface of the flow was densely seeded by aluminum powder clusters with mean size of approximately 0.4 mm. Video images of the tracer field (25 frames per second at resolution of 540×720 pixels) were processed using an interrogation window of 9×9 pixels on an equidistant grid of 54×74 points (grid step is about 2.3 mm in dimensional units). The two analyzed frames were shifted in opposite directions relative to fixed grid points (by some vectors $\mathbf{d}/2$ and $-\mathbf{d}/2$, respectively), and displacements $\mathbf{d}$ were sought at every grid point that minimize absolute difference of image intensities of two frames integrated over the interrogation windows centered around that grid point. This procedure led to the reduced number of erroneous displacement vectors (compared with the standard correlation analysis). Erroneous vectors were discriminated by computing the difference between the displacement vector and the mean displacement over neighbor-
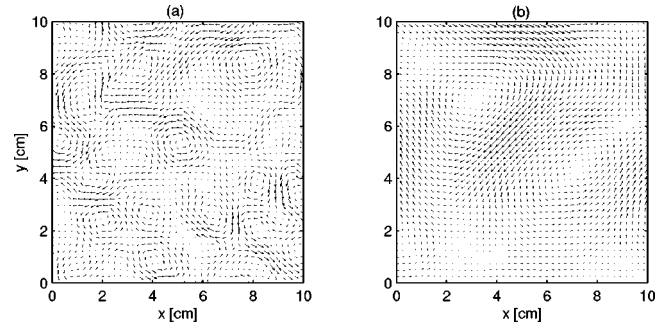

FIG. 1. Fragments of the velocity field in quasistationary phase (a) and at the end of the decay experiment (b). Initial current is 1 A and $h = 5$ mm. Maximum velocities are 3.8 cm/s (a) and 0.07 cm/s (b).

ing points for each grid point, and comparing it with doubled standard deviation over neighboring points (see [21]). The erroneous vectors were replaced by mean displacement over neighboring points. Typically the interrogation window contained images of several tracer clusters.

As the velocity field decays, the fraction of subpixel displacements between two successive frames increases, and consequently, the PIV accuracy drops down. In order to avoid this, we adjusted the time interval between consecutive frames taken for measurements. If rms tracer particle displacement between two given frames became less than some threshold value, the displacement data were discarded and processing was repeated with frames separated by longer time interval. The threshold value was determined experimentally by smoothness of the energy decay curve and was typically less than two pixels. We terminated processing flow images when the time interval between two analyzed frames became some small fraction of the inverse of the instantaneous decay rate. Since velocity field decays nearly exponentially at the final stage, the error due to finiteness of the interval between frames can be estimated analytically and turns quadratic in the time interval between the frames. We neglected these errors as being small.

The restored velocity field contains some "grid" noise that is emphasized in vorticity and divergence fields. We partially suppressed it by computing vorticity and divergence by 8 grid points adjacent to a given one. Although the divergence of the measured velocity field is small, it is finite and its rms value can reach (10–15)% of rms vorticity in experiments with high initial velocity amplitude. As the flow slows down, the ratio of rms divergence to rms vorticity decreases.

Figure 1 shows the velocity field forced by the electric current of 1 A in quasistationary phase (a), and at the end of the decay experiment (b) in a fluid layer with thickness $h = 5$ mm. Only a part of the working domain is shown. The initial field contains vortices of the magnet size and structures of greater size are observed in the final phase. Maximum velocity amplitude is 3.8 cm/s in Fig. 1(a), and 0.07 cm/s in Fig. 1(b). Frames separated by 0.04 and 1.48 s respectively were used to recover these velocity fields.

B. Parameters

The velocity field in a thin-layer flow satisfies the no-slip boundary condition at the cell bottom. This brings about the

bottom drag as an additional dissipation mechanism. Since flows forced electromagnetically are typically slow and approximately two dimensional, the presence of the bottom drag is usually parametrized (see [20]) via a linear drag term in the 2D vorticity equation,

$$\partial \zeta + [\psi, \zeta] = -\lambda \zeta + \nu \Delta \zeta, \tag{1}$$

where ψ is the stream function at the flow surface, $\zeta = \Delta \psi$ the vorticity, $[\psi, \zeta]$ the Jacobian of fields ψ and ζ, ν the kinematic viscosity, and λ the linear drag coefficient. It can be estimated as $\lambda = 2\nu\kappa/h^2$, with κ a fit parameter of order unity. This estimate comes from considering the flow as locally a quasi-Poiseuille one, and the parameter κ accounts for nonuniform vertical profile of the driving force [20,22].

Cardoso *et al.* [19] and Hansen *et al.* [11] suggest that $\kappa = \pi^2/8$, or that λ is the decay rate of the first Stokes mode (a proper value for the decay rate if nonlinear terms are neglected in the equations of motion). Our experience is that κ may admit higher values [22] at the nonlinear stage.

We emphasize that the presence of linear drag is typical for quasi-2D flows studied in laboratory. In experiments with rotating fluids it comes from the Ekman boundary layer (see, e.g., [20]), and in experiments with soap films, as a result of friction against the surrounding air [13,17].

Because of the presence of two dissipation mechanisms, thin-layer flows are characterized by two Reynolds numbers. The first, commonly used Reynolds number is $\mathrm{Re} = UL/\nu$, where U is the velocity scale and L is the typical size. We adopt $U = E^{1/2}$ and $L = (E/Z)^{1/2}$, to obtain $\mathrm{Re} = E/Z^{1/2}\nu$, as in [14]. It should be multiplied with a factor of $2^{1/2}$ to obtain the Reynolds number defined in [10]. Here E and Z are the energy and enstrophy (per unit mass), respectively. For flows with initial energy spectrum concentrated in the vicinity of forcing wave number k_f, the scale L corresponds to k_f^{-1} and is much less [by a factor of $(2\pi)^{-1}$] than the wavelength. While this could cause some inconvenience in comparing L with observed sizes of vortex features, the definition of L in terms of energy and enstrophy is free of conventions that would be necessary otherwise. The same definition of scale is used in [19].

In our experiments $k_f^{-1} = (k_{fx}^2 + k_{fy}^2)^{-1/2} = d/(\pi\sqrt{2})$ or 0.31 cm. Here $k_{fx} = k_{fy} = d/\pi$ are the components of forcing wave number along side walls of the cell and d is the magnet diameter. The estimate for the maximum initial Reynolds number is $\mathrm{Re} \approx 100$, which is also close to the values reported in soap-film experiments (see [13,14] and take into account that the external scale in Ref. [13] is 2π times greater). The Reynolds number defined on the working area (or cell) size is much higher and exceeds 2000 in experiments forced by the current higher than 1 A (papers [11,19] report close values of the cell-size Reynolds number).

The second Reynolds number is based on the bottom drag. It could be defined as $\mathrm{Re}_d = U/L\lambda = Z^{1/2}/\lambda$ and thought of as the number of vortex turnovers performed for linear drag spin down time. This quantity is smaller than the common Reynolds number because the bottom drag in thin-layer flows is responsible for the larger part of dissipation. Flows will be governed by the lowest Reynolds number, thus the
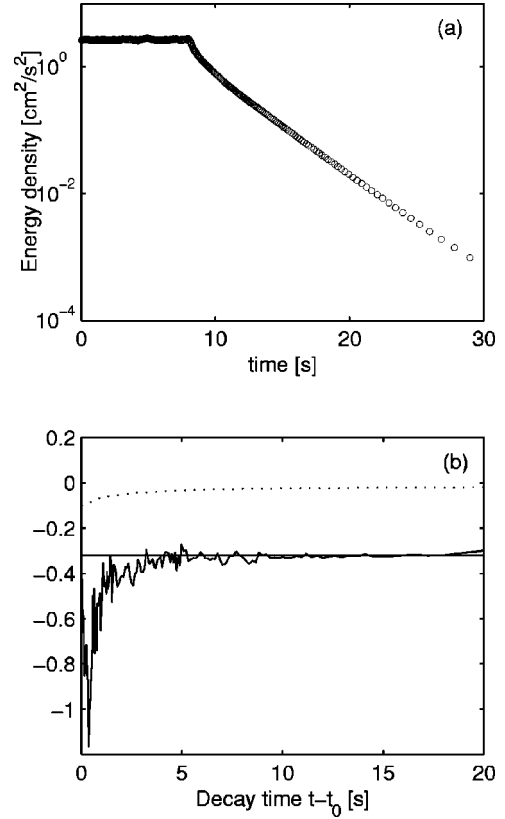

FIG. 2. Energy decay in experiment with $\mathrm{Re}(t_0) \approx 83$ and $h = 5$ mm (a) and contributions to the energy decay (b): $d(\ln E)/dt + 2\nu Z/E$ (irregular solid line), -2λ (straight solid line), and $-2\nu Z/E$ (dotted line).

presence of bottom drag makes them less supercritical and is of primary importance.

To compensate the contribution from the linear drag term in Eq. (1) the authors of [11] propose to make the transform to new, "compressed" time defined as

$$d\tau = e^{-\lambda(t-t_0)}dt,$$

or $\tau = \{1 - \exp[-\lambda(t-t_0)]\}/\lambda$, and to compensated fields $(\psi', \zeta') = (\psi, \zeta)\exp[\lambda(t-t_0)]$. In new variables, the linear drag term disappears and the vorticity equation becomes

$$\partial_\tau \zeta' + [\psi', \zeta'] = \nu' \Delta \zeta'.$$

The price paid for the transform is the exponentially growing viscosity $\nu' = \nu \exp[\lambda(t-t_0)]$ and finite evolution time. While the compressed time could be convenient for the analysis, it requires the experimentally determined parameter λ, and errors in λ would be exponentially amplified in the compensated fields.

C. Energy decay and the drag coefficient

Figure 2(a) shows the typical pattern of energy decay in our experiments. It refers to the flow forced (at $t < t_0$) with the current of 2 A in a layer with thickness $h = 5$ mm. The initial Reynolds number $\mathrm{Re} \approx 83$. Making use of the variable time step between analyzed frames made it possible to ob-

serve energy decay for more than 3 orders of magnitude. As follows from Fig. 2, the energy approximately follows the exponential law for most of the decay. However, closer inspection of energy evolution in experiments with relatively thick fluid layer ($h = 5–6$ mm) shows that the exponent varies during the decay, from larger to lower values. This partly reflects the decrease in the contribution from ordinary viscosity as the typical flow scale grows during decay. In experiments with small h, the exponent remains virtually constant after some initial phase, as the contribution of ordinary viscosity (compared to the bottom drag) into the decay decrement is small even on the energy injection scale.

The energy budget equation for the case under consideration is

$$\dot{E} = -2\lambda E - 2\nu Z + F/S,$$

where $F = -\int_{\partial S} \mathbf{n} \cdot \mathbf{v}(v^2/2 + p/\rho)dl + \nu \int_{\partial S} \zeta \mathbf{v} \cdot d\mathbf{l}$ is the energy flux into the flow through the lateral boundaries, S the area of working domain, $d\mathbf{l}$ is the element of the boundary oriented so that the domain is to the left, and $\mathbf{n}$ is the vector of outer normal. The longer walls of the working domain are rigid and do not contribute to F. The flux through shorter walls is not zero, but could be neglected, as positive and negative contributions effectively cancel each other making F/S very small compared to the total energy dissipation.

Figure 2(b) illustrates the procedure of computation of the drag coefficient λ. The irregular solid line in Fig. 2(b) displays the difference between the full decay rate, given by the logarithmic derivative of energy, $d \ln E/dt$, and the contribution into the decay rate from the ordinary viscosity $-2\nu Z/E$. The latter quantity is plotted by the dotted line for comparison. The data refer to the same experiment as in Fig. 2(a). The logarithmic derivative is computed by forward differences and smoothed using moving mean over three data points (this affects only the initial part of the curve where energy tendency $\dot{E}$ fluctuates noticeably). The straight solid line in Fig. 2(b) corresponds to the mean exponent (determined over last 15 s) of energy decay due to the bottom drag. This exponent is identified with 2λ.

The initial part of the irregular curve goes below the solid straight line, indicating that the energy decay rate $|dE/dt|$ is larger than the sum $2\lambda E + 2\nu Z$, contrary to what one would expect from a strictly 2D flow. The discrepancy between the irregular and straight lines in Fig. 2(b) should be attributed to 3D adaptation of the flow on early stages of the decay. The contribution from ordinary viscosity measures one-fourth of the total 2D decay rate ($2\lambda + 2\nu Z/E$) initially, and drops to less than 1/16 at the end of the experiment. We conclude that the main contribution into the decay rate comes from the bottom drag, and even total neglect for ordinary viscosity would change the value of λ measured in experiment but slightly.

We found that the quantity $\kappa = \lambda h^2/(2\nu)$ slightly decreases as the layer thickness is increased; for a series with the same h it decreases with the Reynolds number. Its averaged value $\kappa = 1.7 \pm 0.15$ for the kinematic viscosity $\nu = 0.012$ cm^2/s. The measured value of κ is different from the values reported in [22] (1.5–1.6), however, it could de-
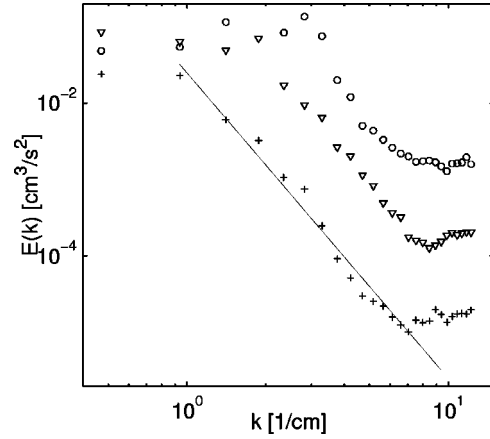

FIG. 3. Evolution of energy spectrum in a flow excited with current of 1 A. $\lambda(t - t_0) = 0$ (○), 0.35 (∇), 1.15 (+).

pend on the flow geometry. It is also higher than the value $\kappa = \pi^2/8 \approx 1.23$ for the first Stokes mode used in Ref. [11]. The latter fact is perhaps not surprising because the flow Reynolds number is greater than unity except for the final phase of the decay experiment. The measured value of λ varies from 0.17 to 0.15 s^{-1} in experiments initially forced with currents from 0.5 to 3 A in a fluid layer of $h = 5$ mm.

D. Decay exponents

We present the analysis of the decaying turbulence as derived from experiments performed with fluid layer of thickness $h = 5$ mm. Figure 3 shows typical evolution of the isotropic energy spectra computed immediately at the beginning of the decay, at $\lambda(t - t_0) \approx 0.35$ and at $\lambda(t - t_0) \approx 1.15$ in the experiment with the initial Reynolds number Re = 55 (initial current of 1 A). The spectra were computed after applying the Hanning window to the velocity field. The spectral shape does not change after $\lambda(t - t_0) = 1.15$ and only the amplitude of the spectrum decreases. The initial spectrum has the peak at $k \approx 2.8$ cm^{-1}, which is close to the forcing wave number k_f estimated above. As the flow decays, energy penetrates to smaller k and the energy peak shifts to the largest resolvable scales. We were not able to study the behavior of the peak wave number as a function of time, as the available spectral range was too narrow and spectral peaks were only marginally seen.

All spectra show saturation at large k, which is the consequence of finite accuracy of the experimental data (cf. [13,15]). The straight thin line in Fig. 3 has a slope of -4. While such a slope does not contradict the available experimental data (a slope of -3.3 was reported in Refs. [12,13,15]), the power-law behavior takes place over very limited wave-number interval that is narrower than in typical soap-film experiments, see Refs. [13,15].

Figures 4(a) and 4(c) show the decay of compensated enstrophy $Z' = (\zeta')^2/2$ and the growth of the typical size $L = (E/Z)^{1/2}$ against the compressed time τ in three realizations with various initial Reynolds numbers. Figures 4(b) and 4(d) show the ratio of enstrophy to energy and the behavior of vorticity kurtosis as functions of the decay time $t - t_0$. The
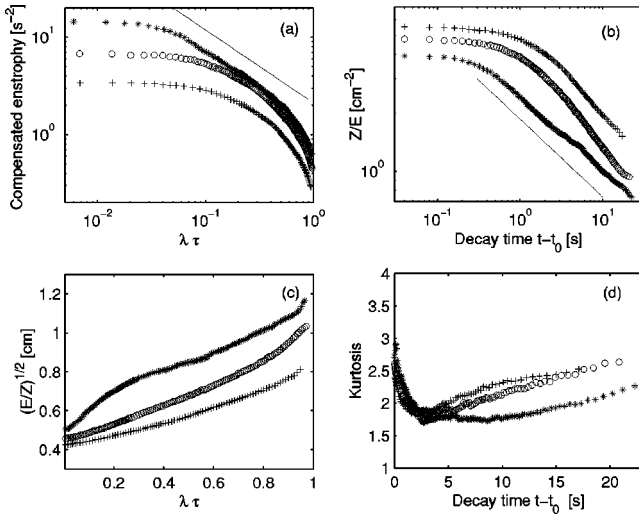
FIG. 4. Compensated enstrophy Z' (a), the ratio of enstrophy to energy (b), typical size $L=(E/Z)^{1/2}$ (c), and kurtosis (d) in decay realizations with different initial Reynolds number. $+$, $\bigcirc$, and $*$ correspond to initial forcing by the currents of 0.5, 1.0, and 3.0 A, respectively; the straight line in (a) has a slope of -0.75, and the straight line in (b) has a slope of -0.4.

three realizations analyzed in Fig. 4 were obtained by transmitting initial currents of 0.5, 1, and 3 A through the electrolyte. Corresponding Reynolds numbers are given in Fig. 5.

All decay realizations excited by currents of the same magnitude show close behavior, although there always are some fluctuations due to different initial conditions.

If we follow the argument of [11] and analyze the decay of compensated enstrophy vs compressed time [Fig. 4(a)], we would conclude that there exists an interval where the compensated enstrophy approximately obeys the power law,

$$Z' \sim \tau^{-\xi_Z},$$

provided that the initial Reynolds number (see Fig. 5) is sufficiently high. The power-law interval is not very wide and disappears altogether as the initial Reynolds number is
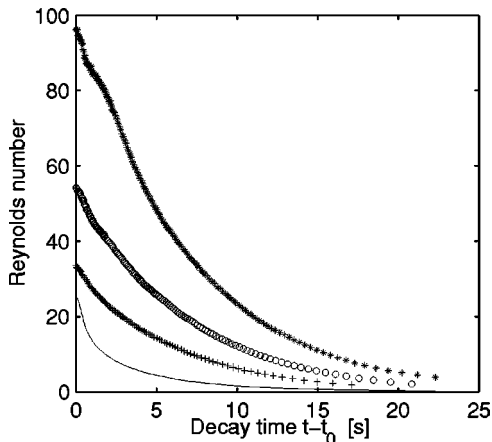

FIG. 5. Reynolds numbers for the experiments shown in Fig. 4 ($+$, $\bigcirc$, and $*$). The thin line plots Re_d corresponding to the case of highest $Re(t_0)$.

decreased. The slope of the thin line in Fig. 4(a) is -0.75. For the experiment with the highest Reynolds number the least square fit gives the spectral slope $\xi_Z=0.77\pm0.035$ over the interval of $\lambda(t-t_0)$ from 0.05 to 0.83, and it becomes 0.95 ± 0.23 for a wider interval from 0.05 to 3.3. It is shallower than the slope reported in Refs. [9,10]. According to [9] $\xi_Z=1.2$, and Ref. [10] gives ξ_Z around 1.2 for the range of Reynolds numbers in our experiments, with $\xi_Z\rightarrow0.8$ in the limit of Re sufficiently large (Re$>1024/2^{1/2}$). However, in our experiments, the Reynolds number (Fig. 5) decreases with time, so one would expect a steeper (if any) exponent.

The observed exponent of the enstrophy decay law also differs from the value reported in Refs. [11]. Hansen *et al.* [11], however, measure the exponent of the decay of the enstrophy-to-energy ratio $Z/E=Z'/E'$. Similarly as with Z', we found Z/E as a function of τ to exhibit a power-law region only in the realization with the highest $Re(t_0)$. The respective exponent is -0.5 ± 0.07 for $\lambda(t-t_0)$ varying from 0.05 to 3.3, close to the value reported in Ref. [11]. The decay exponent determined in this way deviates even further from the theoretical predictions.

The difference between the values of exponents determined by the decays of Z' and Z/E comes entirely from the difference between the bottom drag decay $\exp[-2\lambda(t-t_0)]$ that is compensated in Z', and the real decay of energy (with a contribution from ordinary viscosity and 3D effects). This difference is small at the final stage of the decay, but it is significant initially.

The power-law behavior is expressed much better if we plot Z' or the ratio Z/E against the decay time $t-t_0$. The decay of Z/E is shown in Fig. 4(b). While the slope changes from realization to realization, the power-law behavior is observed for all three cases presented in Fig. 4(b). The thin straight line (drawn for comparison) corresponds to a slope of -0.4. The measured slopes are -0.44 ± 0.03 [time interval $0.2\le\lambda(t-t_0)\le3$], -0.48 ± 0.04 [$0.13\le\lambda(t-t_0)\le3.5$], and -0.37 ± 0.02 [$0.05\le\lambda(t-t_0)\le3.3$] for the realizations initialized with currents of 0.5, 1, and 3 A, respectively. The decay of the compensated enstrophy against ordinary time is characterized by power laws with exponents -0.83 ± 0.03 [time interval $0.27\le\lambda(t-t_0)\le3$], -0.78 ± 0.05 [$0.13\le\lambda(t-t_0)\le3.5$], and -0.71 ± 0.04 [$0.05\le\lambda(t-t_0)\le3.3$] for the same realizations.

We note that the slopes found for enstrophy decay against both the compressed and ordinary times are close. The same conclusion can be drawn from the comparison of the results of [11,19]. The slopes, however, are sensitive to the way in which the influence of the bottom drag is compensated.

Since the typical vortex size as defined here is linked to the enstrophy-to-energy ratio $[L=(Z/E)^{-1/2}]$, the presence of power-law interval in the dependence of Z/E on $t-t_0$ implies the presence of the power-law interval in the dependence of L on $t-t_0$, and exponents can be computed from those of Z/E.

However, if typical vortex size is plotted against the compressed time τ, it shows almost linear behavior in all three cases, see Fig. 4(c). In log coordinates, L as a function of τ would show a power-law interval only for the highest Rey-

nolds number. Since typical vortex size increases only two-fold for the time of evolution, neither of the interpretations is reliable.

The magnitude of vorticity kurtosis [Fig. 4(d)] is below the Gaussian value of 3. It drops at the beginning of the decay to approximately 1.8, but starts to increase afterwards. This suggests that vorticity distribution is rather smooth, and well-pronounced vorticity extrema, or vortices, are not present initially, and do not form as turbulence evolves. Indeed, one would normally associate the appearance of well-formed vortices with high magnitude of kurtosis, up to several tens (see, e.g., [1,7]). This aspect of turbulence evolution in thin layer makes it very different from the evolution observed in numeric simulation.

In all our experiments the Reynolds number (see Fig. 5) decreases down to values of several units (we were unable to follow very small flow velocities down to the complete decay). Plotted as a function of the compressed time, it decreases approximately linearly. The observed decrease in the Reynolds number indicates once again that the decay in thin layers is different from that observed in typical numerical simulations. Indeed, as follows from [10], the decay in a fluid with normal viscosity proceeds with increase of the Reynolds number if initially Re exceeds a value of $15.73/2^{1/2}$. In all cases presented in Fig. 5 the initial Reynolds number is higher than critical, but no increase is observed.

As we have already mentioned, the real role of dissipation is underpredicted by ordinary Reynolds number, and decaying flows enter the stage of linear dissipation earlier than Re becomes comparable to unity. The Reynolds number based on the bottom drag is more appropriate quantity for flows in thin layers. In Fig. 5 we present the evolution of the Re_d for the highest initial Reynolds number (thin line). This quantity is smaller than the ordinary Reynolds number and becomes less than unity 11 s after the beginning of the decay. The subsequent evolution of the flow is linear decay, when nonlinear energy transfer does not play any significant role.

E. Vorticity patterns

The small (smaller than Gaussian) magnitude of kurtosis indicate the absence of strong vortices in vorticity field. Figure 6 presents vorticity realizations at the forced stage (a), 2 s [$\lambda(t-t_0)\approx0.3$] after forcing was switched off (b), and at the final stage of the decay 20 s [$\lambda(t-t_0)\approx3$] later (c) in the experiment with $Re(t_0)\approx83$. Contours in vorticity patterns are drawn at levels of rms and twice rms vorticity ζ_{rms}. The areas where vorticity exceeds $3\zeta_{rms}$ are practically absent. The areas occupied by vorticity in excess of $2\zeta_{rms}$ do not possess regular (circular or elliptic) form, and are surrounded by much wider areas where vorticity level is between one and two rms. These latter seem to be more important dynamically, since they induce larger velocity field than "vortices"—areas with $|\zeta|>2\zeta_{rms}$. The size of vorticity patches increases during evolution, together with the distance between their centers. For example, the number of contours $|\zeta|=\zeta_{rms}$ seen in Fig. 6(a) is approximately five times greater than that in the final pattern in Fig. 6(c).
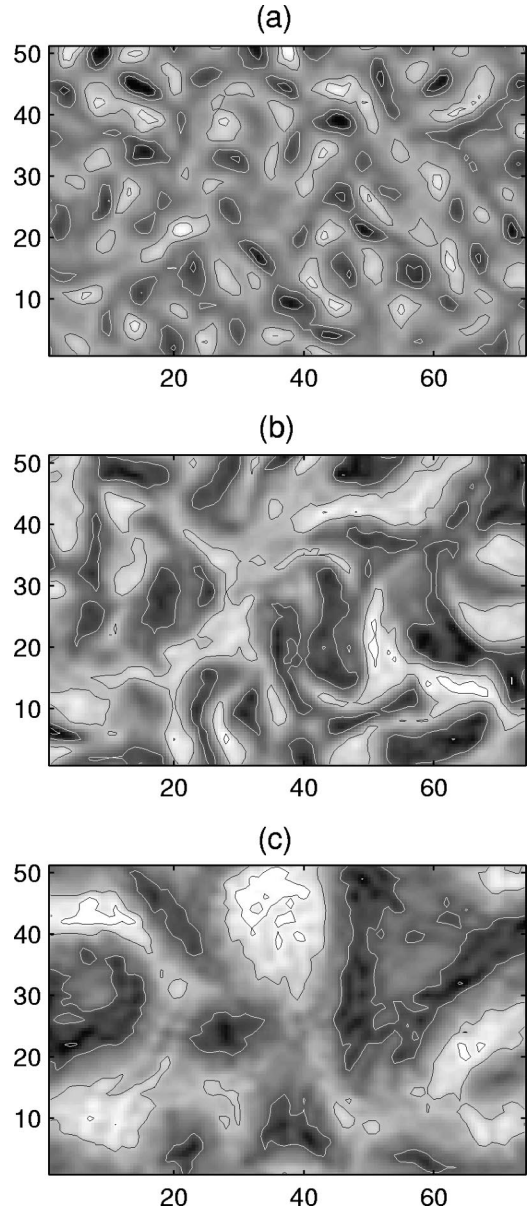

FIG. 6. Vorticity patterns in forced regime (a), 2 s after the beginning of the decay (b), and in the final phase 20 s later (c). The black and white contours correspond to rms and double-rms levels, and the gray scale palette is used. The coordinates are in grid intervals.

However, there is much arbitrariness around any vortex census algorithm in such smooth vorticity fields, and we choose not to speculate on quantities such as the number of vortices or the distance between vortices.

Comparison of Figs. 6(a) and 6(b) shows that initial decay of turbulent flow proceeds as one would have expected. The vortices stretch each other and the population of initial vorticity patches evolves into filaments. Still, in one respect, the vorticity pattern looks very different from that seen in numerical simulations. We do not observe thin and intense filaments and typical filament thickness is limited to several grid intervals. Instead of intense stretching, formation of very elongated structures, and appearance of strong vortices on

such a background, we observe rather "smooth" decay, and the area where vorticity level exceeds ζ_{rms} occupies a considerable part of the total area during the decay. The final vorticity distribution, Fig. 6(c), consists of wide vorticity patches, and contours $|\zeta| = \zeta_{rms}$ look very irregular. This indicates that we are dealing with remnant vorticity that slowly dies away. The distribution of vorticity in Fig. 6(c) contains fluctuations on the grid scale—they are seen because of the very low vorticity amplitude.

III. DISCUSSION AND CONCLUSIONS

According to the results presented above, the enstrophy decay in thin-layer flows could be approximated by power laws $(t-t_0)^{-\xi}$ over some interval of decay time $t-t_0$. However, the value of the decay exponent proves sensitive to the way in which it is determined. The problem comes from the influence of bottom drag that introduces additional dissipation of both energy and enstrophy as $e^{-2\lambda(t-t_0)}$. If this dissipation is compensated directly by introducing the compensated enstrophy Z', we find ξ scattered around 0.75 depending on the initial Reynolds number. If the bottom-drag dissipation is "compensated" by considering the enstrophy-to-energy ratio, the exponent is around a value of 0.45, in agreement with the results previously reported in Refs. [11,19]. Using the compressed time instead of ordinary time makes the performance of power-law approximation worse, as the decay curve becomes steeper as $\lambda\tau \rightarrow 1$.

However, both Z' and Z/E (independent of the time scale used) do not seem to be proper quantities for the comparison with numerical simulations. Indeed, in numerical simulations of decaying 2D turbulence (see, e.g., [7]) the energy remains virtually constant during the decay. On the contrary, in laboratory experiments that use thin-layer setups, the energy essentially decays, mostly due to the bottom drag, but also due to the ordinary viscosity, since the initial Reynolds number is not very high. The 3D adaptation at the initial stage reduces the Reynolds number even further. Our conclusion is that one cannot compare these cases, and the fact that the slope of enstrophy decay is sensitive to the type of compensation supports it.

We do not see any developed vortices in the evolving vorticity field, and the vorticity kurtosis remains less than the Gaussian value of 3 (the same is true for [11], see their Fig. 8). This should be compared to a value of several tens typical to the numerical decay simulations [1,7]. The dynamics of the vorticity field in decaying turbulent thin-layer flows do not reduce to the dynamics of point vortices, so we cannot expect that it would follow the scenario of [3] (at least at current values of the Reynolds number). Even if we leave aside the obvious influence of bottom drag, the decay should be sensitive to the type of small-scale dissipation and the Reynolds number, as we have already mentioned in the Introduction.

In accordance with the modified vorticity equation (2), the decay of thin-layer flows vs the compressed time is accompanied by increase of ordinary viscosity. This results in decreasing Reynolds number at large time, so the self-similar decay is hardly possible. However, one would expect that in this case the compensated enstrophy would decay faster than power -0.8 (the shallowest value of the decay exponent in [10]) of the compressed time τ. So the question is why the compensated enstrophy decays anomalously slowly in the experimental system studied here. The answer could be the absence of thin vorticity filaments in the vorticity field and thus the suppression of the enstrophy cascade to smaller scales. This corresponds to relatively small effect of advection compared to that of dissipation, or in other words, to the initial Reynolds numbers being insufficiently high due to the presence of bottom drag. The fact that flows in thin layers are two dimensional only, approximately, and two dimensionality is broken on scales comparable to or less than the fluid depth, could also play some role. The true enstrophy dissipation is influenced by 3D processes and need not obey 2D equations.

The peculiar feature of flows excited electromagnetically in thin layers is that the horizontal scale of forcing is typically close to or larger than the fluid layer thickness, as thick layers cannot be excited effectively due to an exponential decay of the magnetic field with distance from the bottom. This results in strong bottom drag compared to ordinary dissipation, and relatively high initial Reynolds numbers are needed to provide a time interval with the Reynolds number growing during the decay. In this respect soap-film setups are less restrictive, and the growth of the Reynolds number in decaying soap-film turbulence was already reported in Ref. [13]. In Ref. [13], the initial Reynolds numbers are of the same order as in our experiments (their integral scale is 2π times higher), the energy and rms velocity are decaying due to external drag, but the integral scale is growing such that the Reynolds number does not decrease.

[1] J. C. McWilliams, J. Fluid Mech. **146**, 21 (1984).

[2] J. C. McWilliams, J. Fluid Mech. **219**, 361 (1990).

[3] G. F. Carnevale, J. C. McWilliams, Y. Pomeau, J. B. Weiss, and W. R. Young, Phys. Rev. Lett. **66**, 2735 (1991).

[4] J. B. Weiss and J. C. McWilliams, Phys. Fluids A **5**, 608 (1993).

[5] R. Benzi, S. Partanello, and P. Santangelo, J. Phys. A **21**, 1221 (1988).

[6] R. Benzi, M. Colella, M. Briscolini, and P. Santangelo, Phys. Fluids A **4**, 1036 (1992).

[7] A. Bracco, J. C. McWilliams, G. Murante, A. Provenzale, and J. B. Weiss, Phys. Fluids **12**, 2931 (2000).

[8] G. K. Batchelor, Phys. Fluids Suppl. **12**, 233 (1969).

[9] P. Bartello and T. Warn, J. Fluid Mech. **326**, 357 (1996).

[10] J. R. Chasnov, Phys. Fluids **9**, 171 (1997).

[11] A. E. Hansen, D. Marteau, and P. Tabeling, Phys. Rev. E **58**, 7261 (1998).

[12] H. Kellay, X. L. Wu, and W. I. Goldburg, Phys. Rev. Lett. **74**, 3975 (1995).

[13] B. K. Martin, X. L. Wu, W. I. Goldburg, and M. A. Rutgers, Phys. Rev. Lett. **80**, 3964 (1998).

[14] M. Rivera, P. Vorobieff, and R. E. Ecke, Phys. Rev. Lett. **81**, 1417 (1998).

[15] A. Belmonte, W. I. Goldburg, H. Kellay, M. A. Rutgers, B. Martin, and X. L. Wu, Phys. Fluids **11**, 1196 (1999).

[16] H. Kellay, C. H. Bruneau, and X. L. Wu, Phys. Rev. Lett. **84**, 1696 (2000).

[17] M. Rivera and X. L. Wu, Phys. Rev. Lett. **85**, 976 (2000).

[18] A. Belmonte, B. Martin, and W. I. Goldburg, Phys. Fluids **12**, 835 (2000).

[19] O. Cardoso, D. Marteau, and P. Tabeling, Phys. Rev. E **49**, 454 (1994).

[20] F. V. Dolzhanskii, V. A. Krymov, and D. Yu. Manin, Sov. Phys. Usp. **33**, 495 (1990).

[21] M. Raffel, C. E. Willert, and J. Kampenhaus, *Particle Image Velocimet. A Practical Guide* (Springer-Verlag, Berlin, 1998).

[22] F. V. Dolzhanskii, V. A. Krymov, and D. Yu. Manin, J. Fluid Mech. **241**, 705 (1992).